

# Different Geometry Design Structures of Tissue Scaffolds for Additive Manufacturing

**Amir Hossein Ehsani**

Department of Mechanical Engineering,  
Science and Research Branch, Islamic Azad University, Tehran, Iran  
E-mail: ah.ehsani@srbiau.ac.ir

**Sadegh Rahmati\* Mohammad Nikkhoo**

Department of Biomedical Engineering,  
Science and Research Branch, Islamic Azad University, Tehran, Iran  
E-mail: srahmati@srbiau.ac.ir , m.nikkhoo@srbiau.ac.ir

\*Corresponding author

**Shahram Etemadi Haghighi**

Department of Mechanical Engineering,  
Science and Research Branch, Islamic Azad University, Tehran, Iran  
E-mail: setemadi@srbiau.ac.ir

**Mohammad Haghpanahi**

Biomechanics Group, Department of Mechanical Engineering,  
Iran University of Science and Technology, Tehran, Iran  
E-mail: mhaghpanahi@iust.ac.ir

**Received: 27 July 2021, Revised: 15 September 2021, Accepted: 21 September 2021**

**Abstract:** The design and manufacturing cubic porous scaffolds are a considerable notion in tissue engineering (TE). From Additive manufacturing (AM) perspective, it has attained high appeal in the string of TE during the past decade. In the view of TE, the feasibility of manufacturing intricate porous scaffolds with high accuracy contrast to prominent producing methods has caused AM the outstanding option for manufacturing scaffold. From design perspective, porous scaffold structures play a crucial task in TE as scaffold design with an adequate geometries provide a route to required strength and porosity. The target of this paper is achieve of best geometry to become an optimum mechanical strength and porosity of TE scaffolds. Hence, the cubic geometry has been chosen for scaffold and Cube, Cylinder and Hexagonal prism geometries have been selected for pore of structures. In addition, for noticing the porosity effects, pore size has been chosen in three size, and a whole of nine scaffolds have been designed. Designed scaffolds were generated using Fused Deposition Modeling (FDM) 3D Printer and dimensional specifications of scaffolds were evaluated by comparing the designed scaffolds with Scanning Electron Microscope (SEM). The samples were subjected to mechanical compression test and the results were verified with the Finite Element Analysis (FEA). The results showed that firstly, as the porosity increases, the compressive strength and modulus of elasticity obviously decreased in all geometry pore scaffolds. Secondly, as the geometry changes in similar porosity, cubic pore scaffold achieved higher compressive strength and modulus of elasticity than cylinder and hexagonal prime. Experimental and FEM validated results proposed a privileged feasible pore geometry of cubic scaffold to be used in design and manufacturing of TE scaffolds.

**Keywords:** Cubic Scaffold, Pore Geometry, Tissue Engineering, Additive Manufacturing, Mechanical strength, Finite Element Analysis

**How to cite this paper:** Amir Hossein Ehsani, Sadegh Rahmati, Mohammad Nikkhoo, Shahram Etemadi Haghighi and Mohammad Haghpanahi, "Different geometry design structures of tissue scaffolds for additive manufacturing" , Int J of Advanced Design and Manufacturing Technology, Vol. 14/No. 4, 2021, pp. 91-104.  
DOI: 10.30495/admt.2021.1936526.1298

**Biographical notes:** **Amir Hossein Ehsani** is PhD student of Mechanical Engineering Dept. at the Science and Research Branch, IAU University, Tehran, Iran. He received his MSc in Mechanical Engineering from IAU, Semnan Branch, Iran in 2011. **Sadegh Rahmati** is Assistant Professor at the Department of Biomedical Engineering, at the Science and Research Branch, IAU University, Iran. He received his PhD in Manufacturing Engineering from University of Nottingham, England in 1999. **Mohammad Nikkhoo** is Associate Professor of Biomechanical Engineering at the Science and Research Branch, IAU University, Iran. He received his PhD in Mechanical Engineering from IUST, Iran in 2012. **Shahram Etemadi Haghighi** is Associate Professor of Mechanical Engineering at the Science and Research Branch, IAU University, Iran. He received his PhD in Mechanical Engineering from Sharif University of Iran in 2010. **Mohammad Haghpanahi** is Professor of Mechanical Engineering at the IUST University, Iran. He received his PhD in Mechanical Engineering from ENSAM University of France in 1996.

---

## 1 INTRODUCTION

---

1- The rapidly growing discipline of tissue engineering is one of the most hopeful approaches for developing engineered substitutes for damaged bone [1]. Scaffolds for tissue engineering (TE) applications are anticipated to have certain properties to avoid bone loss and encourage bone regeneration. Scaffolds are highly porous structures with interconnected pores. They should ideally be biocompatible, mechanically reliable, biodegradable, osteoconductive, and biomimetic [2–4]. Some important features of a good scaffold are: regular and controlled structure, having the mechanical strength and porosity in the range of cancellous bone, having interconnected pores with appropriate size, high penetration in internal structure, and manufactured with biocompatible material in order to comfort with biology features of bone tissue [5-7]. Many experts believe that the progress of TE is seemingly associated with the improvements in scaffold technology [8].

2- Numerous multidisciplinary studies have been carried out in this field, from design and modelling to material processing [9]. Various processing techniques, such as foam replica [10], freeze casting [11], gas foaming [12], electrospinning [13], and salt leaching [14], have been used to fabricate scaffolds. However, most of these methods cannot fully control the structural properties and reproducibility of the scaffolds. Also, in these methods, due to the random construction in the scaffold, the properties differ in different locations of the scaffold [15]. Today, Additive Manufacturing (AM) allow complex structures designs to be accurately produced at microscopic (100 nm to 100  $\mu\text{m}$ ) spatial length scales [16].

As a result, the use of AM technology and a 3D printer is a long step to construct a structured scaffold with controlled geometry [17]. Among the various incremental manufacturing methods, the Fused Deposition Modelling (FDM) method, FDM is the process of forming a three-dimensional object of predetermined design, and in particular the making of a model or article by depositing multiple layers of a material in a fluid state onto a base. It accomplishes this by converting a CAD-generated 3D model into a cross-sectioned 2.5D model via “slicer” software and fabricated layer by layer by extruding filament through a heating element that can move freely through the XY plane [18, 19]. Due to its Poly Lactic Acid (PLA) filament with biocompatible grades is a safe way to build a BTE scaffold. In this way, the variety of material and geometry is high and many complex geometries may be used to manufacture a BTE scaffold.

Different methods have been developed to design a tissue scaffold in previous researches. The first strategy is to use an MRI image and extract the microstructure of the bone tissue, where the design of a tissue scaffold is in accordance with bone tissue. The advantage of this method is that the

mechanical strength and porosity of the designed scaffold to be consistent with the desired bone tissue, but the disadvantage is that existing fabrication methods are not capable of constructing such a structure [20]. Another strategy is to use simple periodic shapes like cube or sphere to design a scaffolding structure. The advantage of this method is the ease of design and construction and the weakness of this method is the frame of the unit-cell [21, 22]. 3- In this research, the purpose was to investigate the relationship between geometrical characteristics (geometry, porosity, pore size) of porous cubic scaffolds, as well as their mechanical strength to show that the pore geometry may play an important role in mechanical strength of scaffold. Many researchers in recent years by considering changes in construction parameters such as layer thickness, delay time, orientation and other cases, as well as in some articles changes in materials, scaffold porosity and scaffold architecture, have investigated the mechanical properties and strength of scaffolds.

The important point is that none of the researches has mentioned the geometric changes of the unit-cell so far [23-28]. Hence, design and manufacture of different geometries for structure also experimental compression test and fully FEM analyse are novelty of this work. As a result to achieve this, first three models of the pore geometry (Cube, Cylinder and Hexagonal prism) were designed with different sizes due to obtain the effect of porosity on mechanical strength of cubic TE scaffolds. Then the designed scaffolds were fabricated with FDM 3D printer and in order to compare dimensional features, samples were evaluated with scanning electron microscope. In the following, specimens are subjected to mechanical compression test and the results are validated with the finite element analysis.

---

## 2 EXPERIMENT

---

### 2.1. Modelling and 3D-printing of Porous Scaffolds

To achieve different geometries, pores were designed in Cube, Cylinder and Hexagonal prism and scaffold was selected cubic because it deputed the typical architecture and features of a TE scaffold remarked to repair an anatomical deficiency in a biological environment [31]. Porous cubic structures, 18 mm in height and 7.976 mm in diameter, were designed (“Fig. 1”). Also, the pore sizes in all three pore geometries (cube, cylinder and hexagonal prime) were calculated so that the volume of the pore’s unit-cell in each geometry was equal due to the appropriate comparison for porous scaffolds (“Table 1”). Howbeit, the explanation of appropriate pore size of unit-cell is still a subject of discussion [29], it is generally agreed to be in the range of 250–1200  $\mu\text{m}$  [30].

All models are implemented by CAD software (CATIA V5R21), and a total of nine cubic scaffolds have been designed (“Fig. 2”). The parametric design features of the

software give clearance to precisely control the structural parameters of the model, and also allow to measure the porosity of the model, where the porosity P of each model is calculated by equation (1).

$$P = V_p / V \tag{1}$$

Where, P, V<sub>p</sub>, and V are porosity, volume of the porous scaffolds, and outer volume of the porous scaffolds (“Fig. 3”).

The CAD files exported as STL format were imported to a commercial (VAGLER V-8E) 3D Printer. Also, Poly Lactic Acid (PLA) filament with biocompatible degree and proper mechanical properties was considered. PLA has emerged as an important polymeric material for biomedical applications on account of its properties such as biocompatibility, biodegradability, mechanical strength and process ability. PLA is thus an eco-friendly nontoxic polymer with features that permit use in the human body [31]. The slicing software was Cura 0.1.5. All the specimens were fabricated with constant printing parameters, which are provided in Table 2. Moreover, SEM (Tescan Mira3, Australia) images were captured to illustrate more details of the printed scaffolds compared with designed scaffolds.

Table 1 presents that the pore of the porous scaffolds has different size and geometry (Cube, Cylinder and Hexagonal prism) and for effect of porosity consideration, three pore

sizes for any geometry are defined. Previous researchers have shown that a proper pore size for bone cell growth is 200 to 1200 μm [34]. The pore sizes of the nine porous cubic scaffolds are shown in Table 1 and all pore sizes are in proper range (200–1200 μm) for bone cell growth. In general, as increasing pore sizes the porosity of the scaffold increases.

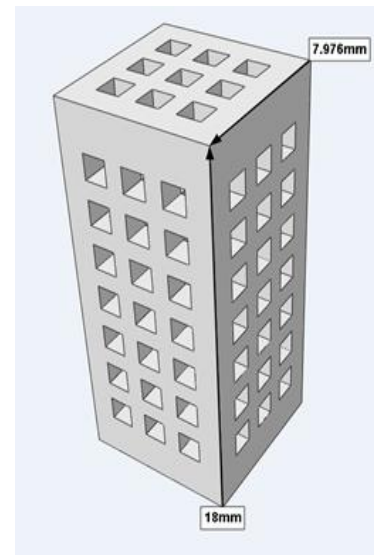
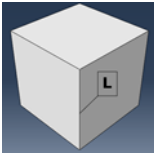
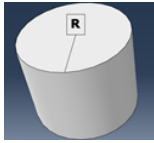
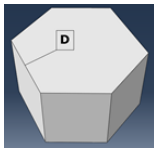
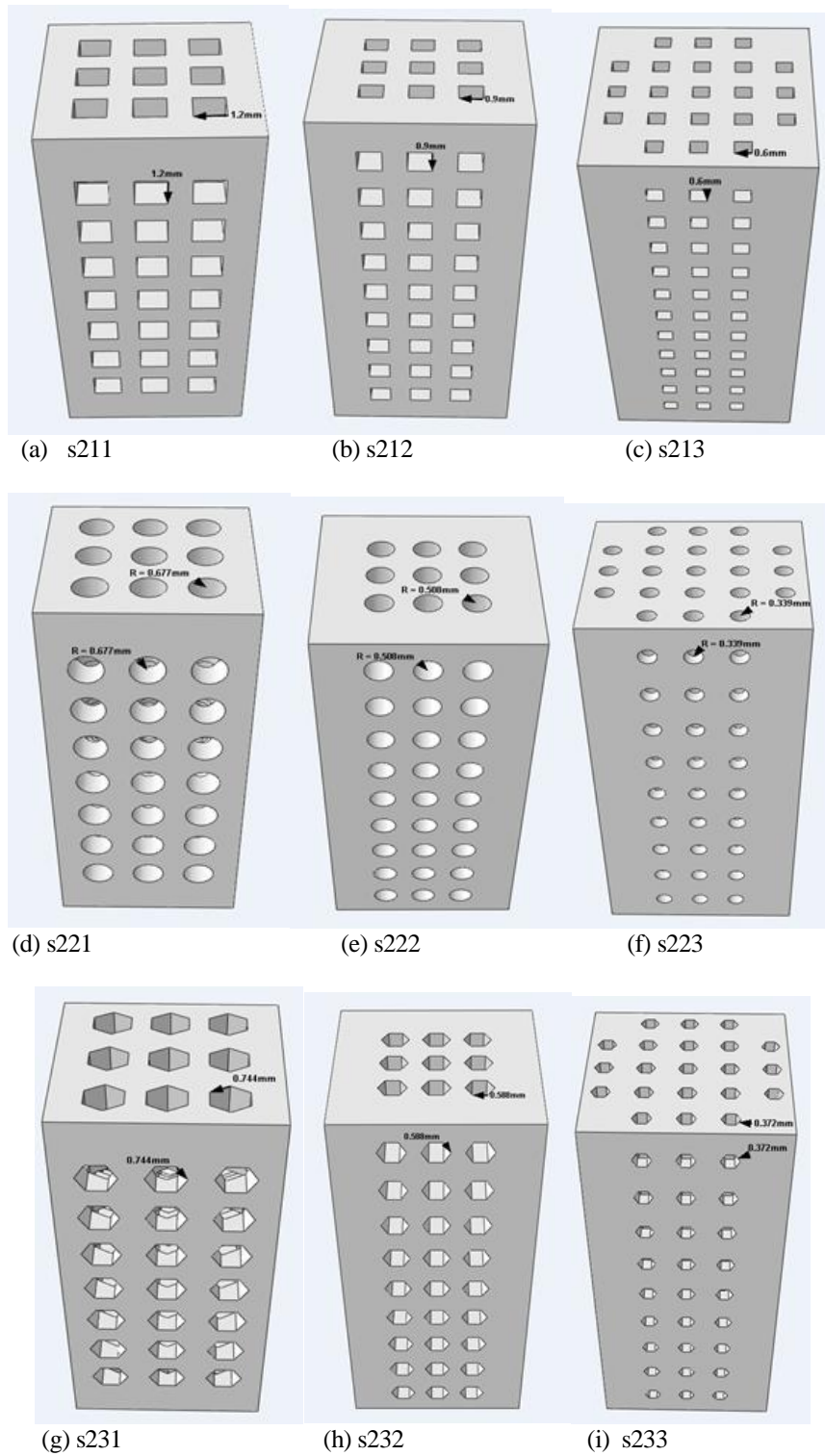


Fig. 1 Structural details of the porous cubic.

Table 1 Pore details of the porous cubic scaffold

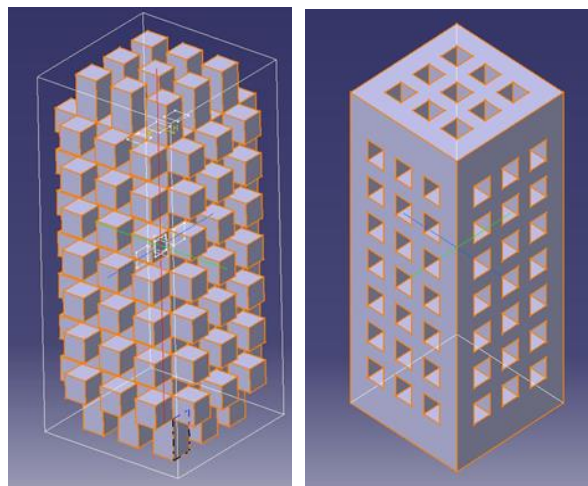
Pore geometry	Pore 3D	Pore size (mm)	Volume (mm <sup>3</sup> )	Symbol
Cube		L1 = 1.2	1,728	S211
		L2 = 0.9	0,972	S212
		L3 = 0.6	0,432	S213
Cylinder		R1=0.68	1,728	S221
		R2= 0.97	0.972	S222
		R3=0.34	0,432	S223
Hexagonal		D1=0.74	1,728	S231
		D2=0.56	0,972	S232
		D3=0.37	0,432	S233



**Fig. 2** Nine porous cubic scaffolds with different pore geometry.

The porosity of the nine porous cubic scaffolds was calculated by equation (1) and shown in Table 3. In order to compare the results between the three types of pore

geometry, the scaffolds design was considered such a way that the volume of scaffolds remained constant in each pore geometries.



(a): volume of the porous cubic scaffolds( $V_p$ ) (b): outer volume of the porous cubic scaffolds( $V$ )

Fig. 3 different volumes of porous cubic scaffold.

Parameter	Value
Infill ratio(%)	90
Nozzle diameter (mm)	0.4
Printing Temperature (oC)	205
Printing speed (mm/s)	50
Printing pattern	Rectangular
Raster angle	45
Layer height (mm)	0.1

As can be seen from “Fig. 4”, s211, s221 and s231 with pore geometry cube, cylinder and hexagonal prime, respectively, have porosity of nearly 45% and s212, s222, s232 with pore geometry cube, cylinder and hexagonal prime respectively, have porosity of nearly 36% and finally s213, s223, s233 with unit-cell geometry cube, cylinder and hexagonal prime respectively, have porosity of nearly 23%. It should be noted that slight differences were due to design considerations.

The 3DP porous scaffolds were fabricated based on nine porous cubic scaffolds with three different porosities in the three geometries of cube, cylinder and hexagonal prime (“Fig. 5”). The nine fabricated porous cubic scaffolds by FDM were compared to their CAD models with respect to their dimensions to evaluate the manufacturing accuracy.

Table 3 Porosity of the porous cubic scaffolds

Scaffold	Porosity(%)
S211	45
S212	36
S213	23
S221	44
S222	33
S223	23
S231	44
S232	36
S233	21

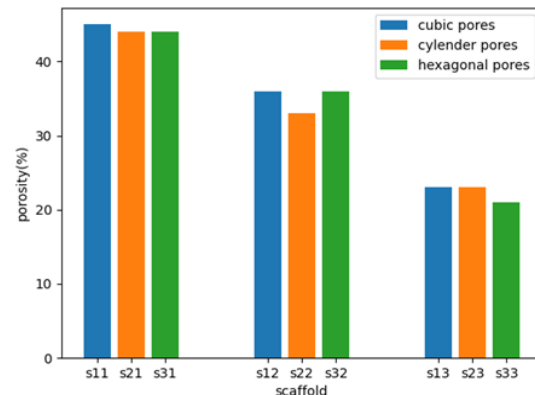


Fig. 4 Porosity of the samples at three different porosities.

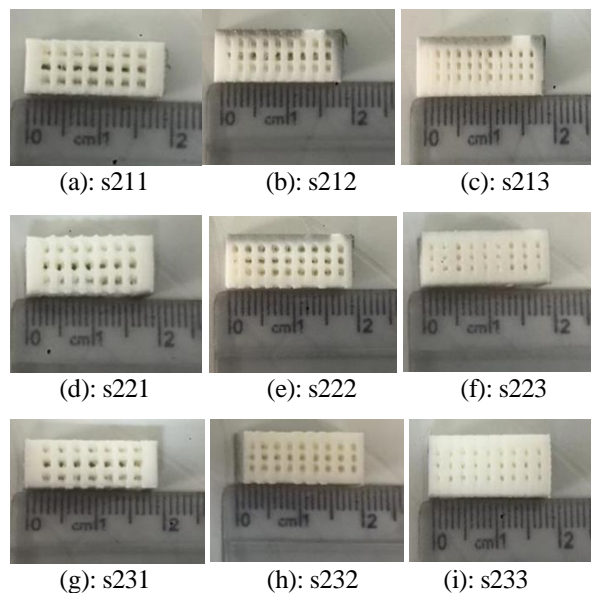
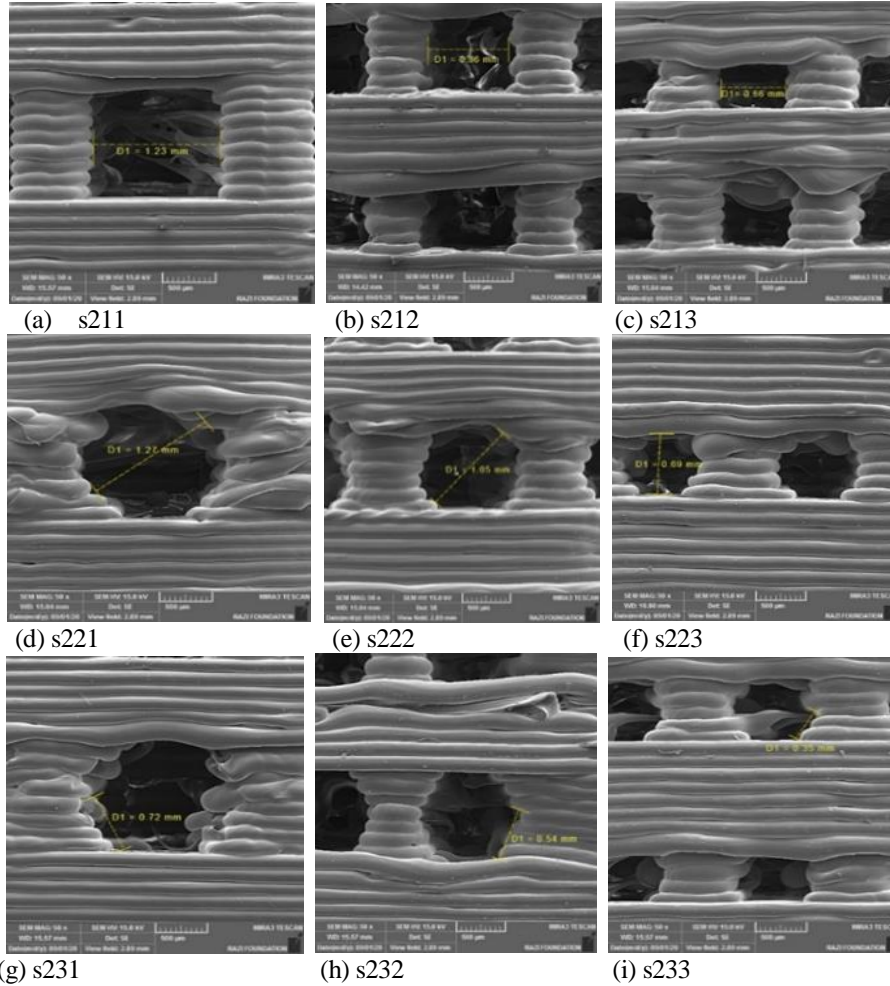


Fig. 5 Fabricated porous cubic scaffolds by FDM.

Figure 6 shows SEM images of size and geometry of pores for nine porous scaffolds. As can be seen, all the nine fabricated scaffolds by FDM were consistent with designed scaffolds in terms of geometry and dimension. Table 4

shows detailed dimensional measurement data porous structures. The results showed that the deviation from designed and fabricated dimension average is negligible.



**Fig. 6** SEM images of the microstructure of the 3DP scaffolds.

**Table 4** Deviation between designed and fabricated dimension

Scaffold	Pore size (mm)		Deviation (%)
	Designed	Fabricated	
S211	1.2	1.23	3
S212	0.9	0.86	4
S213	0.6	0.66	6
S221	0.68	0.64	4
S222	0.51	0.52	1
S223	0.34	0.34	0
S231	0.74	0.72	2
S232	0.56	0.54	2
S233	0.37	0.35	2

### 3 MECHANICAL TEST

Mechanical compressive tests were performed in order to extract the mechanical strength of designed scaffolds. ASTM D695-02a Standard Test Method for Compressive Properties of Rigid Plastics [32] was followed in the tests carried out. Three specimens were manufactured of each scaffold model with the same processing parameters. In order to prevent the anisotropic effects when comparing the structures, all the specimens were exposed to loading parallel to the printing direction.

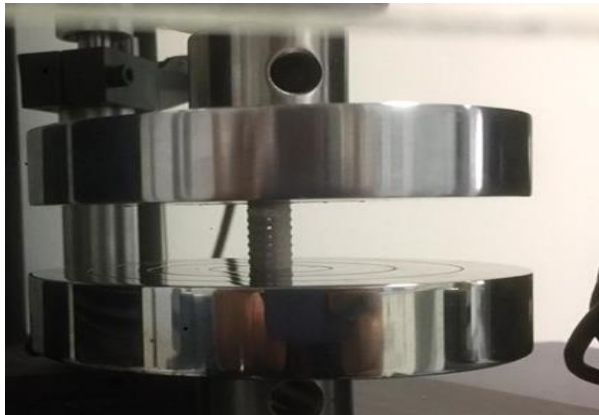
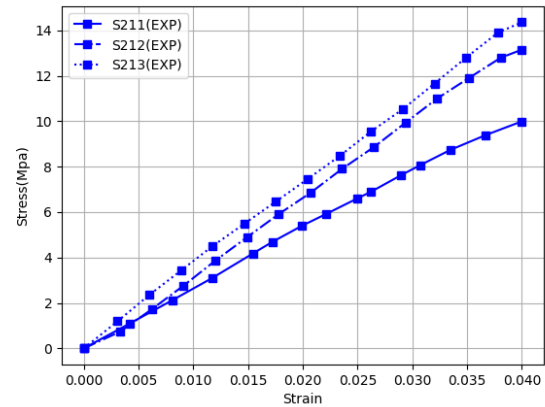


Fig. 7 Uniaxial compression test on a sample by SANTAM device.

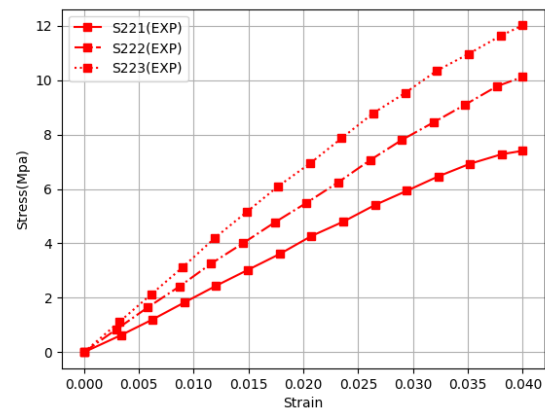
Uniaxial compression tests were performed on a universal testing instrument (Table top STM-20, Santam, Iran) equipped with a 100 KN load cell and a cross-head loading rate of 1 mm min<sup>-1</sup> (“Fig. 7”). Load-displacement data were extracted to calculate engineering stress-strain plot. Then, the graphs were modified according to the onset of elastic region and mechanical properties were computed. Elastic modulus and compressive strength were calculated according to the slope of the first linear region in stress-strain plots (strain from 0 to 0.004 mm/mm) and the maximum recorded stress, respectively.

The graphs were obtained from the force-displacement data recorded during the compressive test. Figure 8 shows the trend of the stress–strain curves of porous cubic scaffolds under same pore geometry and different porosity conditions.

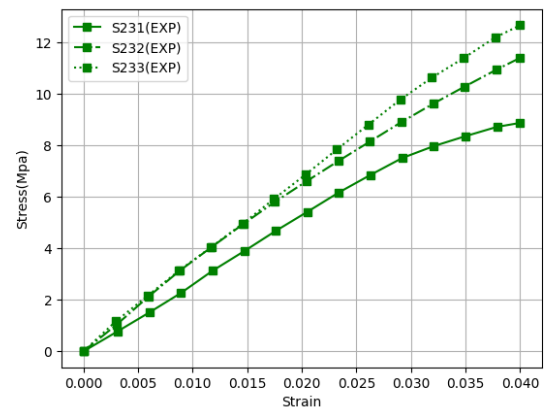
Figure 9 shows the trend of the stress–strain curves of porous scaffolds under different pore geometry and same porosity conditions. Finally, Figure 10 shows the stress–strain curves, overlapped for all specimens.



(a) Cube pore



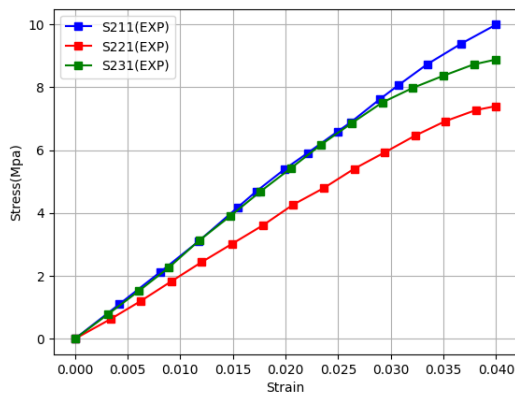
(b) Cylinder pore



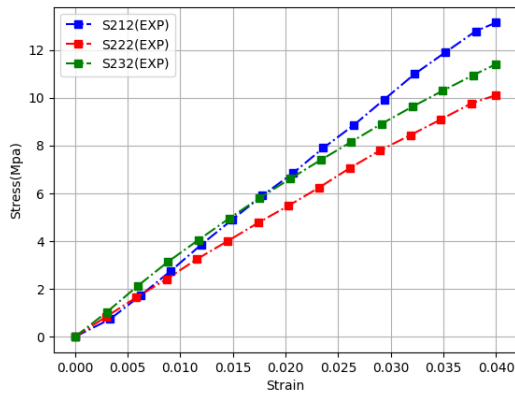
(c) Hexagonal prism pore

Fig. 8 Compressive stress–strain diagrams for same geometries and different porosities.

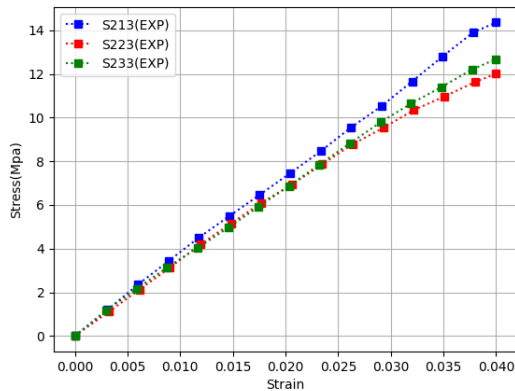
As can be seen from figures, seemingly, the strength has increased in the plastic area of the material. Since, as a consequence of compression, transformations occurred in the material, porosity was reduced, volume decreased and density increased. When the internal structure of the material changed, the load capacity changed. In spite of this, this did not affect the computed parameters.



(a) 44% porosity



(b) 36% porosity



(c) 23% porosity

Fig. 9 Compressive stress–strain diagrams for same porosities and different pore geometries.

As a result, the following corrections were done to the data sets of the compressive tests:

Firstly, the descriptions of stress and strain true values were substituted with their nominal amounts. Hence, during the compressive tests to investigate the variation of the cross section, the constant volume theory was assumed. Secondly, before calculating modulus of elasticity from stress-strain curves, it was necessary to make a correction to the curves to eliminate the effect of toe compensation as followed from annex A1 of standard D695-02a [32, 35].

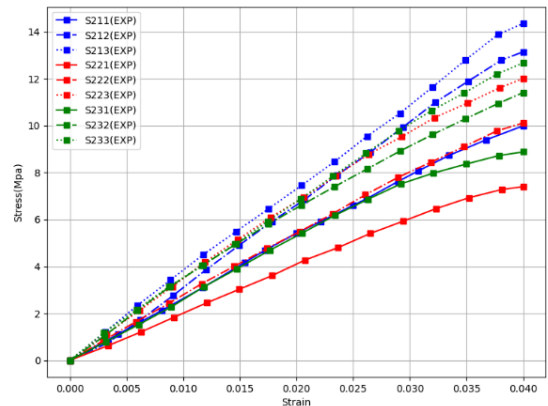


Fig. 10 Compressive stress–strain curves for all specimens.

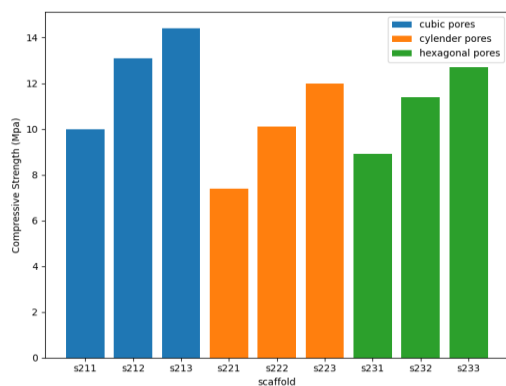
As can be seen from “Fig. 8”, which considers the Compressive stress–strain diagrams for similar geometry and different porosities, as the porosity decreases, the compressive strength of the porous scaffolds increases. Also, as can be seen from “Fig. 9”, which considers the Compressive stress–strain diagrams for similar porosity and different geometries, cubic pore scaffolds have the largest compressive strength than cylindrical and hexagonal prime ones.

Table 5 Mechanical properties from compression test (ASTM D695)

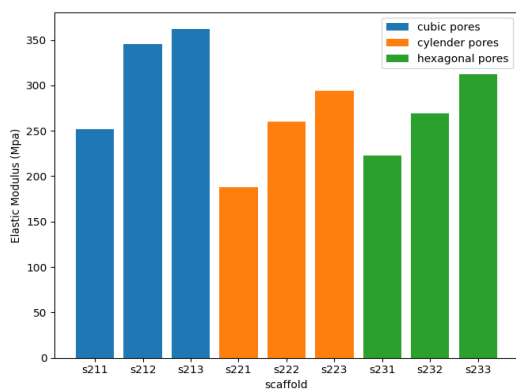
Scaffold	E (Mpa)	$\sigma$ (Mpa)
S211	252	10
S212	346	13.1
S213	362	14.4
S221	188	7.4
S222	260	10.1
S223	294	12
S231	223	8.9
S232	269	11.4
S233	312	12.7



Figure 10 shows that cubic pore scaffolds with 23% and 33% porosity (s213 and s212), have the highest compressive strength with 14.4 Mpa and 13.1 Mpa respectively. Ultimate compressive strength and compressive elastic modulus were calculated using the maximum compressive stress recorded in the stress-strain curve and the slope of the linear area before the yield point. However, values of compressive elastic modulus (E) and compressive strength ( $\sigma$ ) are shown in Table 5. It was noticeable that all the results obtained in compression test were in range of bone mechanical property for TE [36]. As seen in “Fig. 11”, which considers the comparison of compressive strength and modulus of elasticity (E) for nine porous cubic scaffolds, in similar porosities, higher compressive strength and modulus of elasticity were found in the cubic pore scaffolds. Also as the porosity decreases, the modulus of elasticity of the porous scaffolds increases.



(a) Comparison of compressive strength of porous cubic scaffolds



(b) Comparison of modulus of elasticity of porous cubic scaffolds

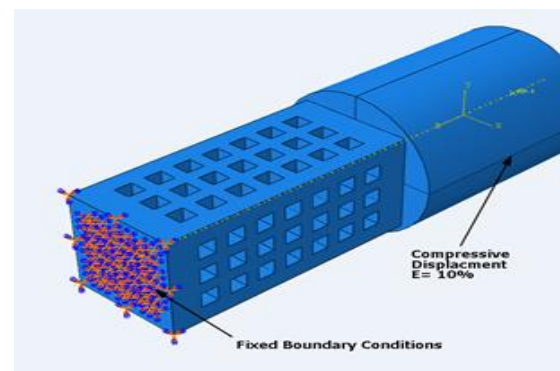
**Fig. 11** Comparison of mechanical properties in compression tests.

As concluded, in similar porosities, cubic pore scaffolds (s211, s212 and s213) showed higher compressive

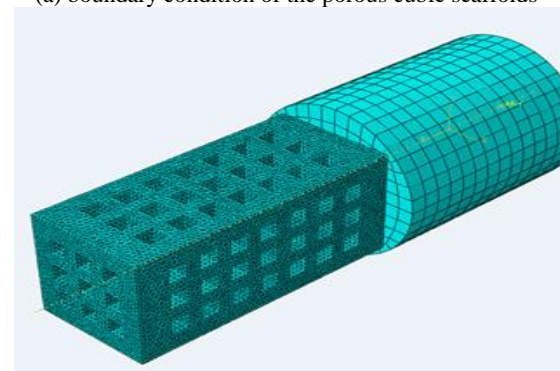
strength than the cylindrical and hexagonal ones. Consequently, the use of cubic pore scaffolds to reach higher compressive strength and modulus E is recommended.

#### 4 NUMERICAL SIMULATION

FEA (Abaqus 6.14, Dassault System, SIMULIA) was performed for each porous cubic scaffolds. The STP model file obtained by CATIA software first generates body mesh in Abaqus software. Finally, three-node Tet element were formed, and the element side length for the 3D mesh was set as 0.3mm for all nine porous scaffolds types.



(a) boundary condition of the porous cubic scaffolds

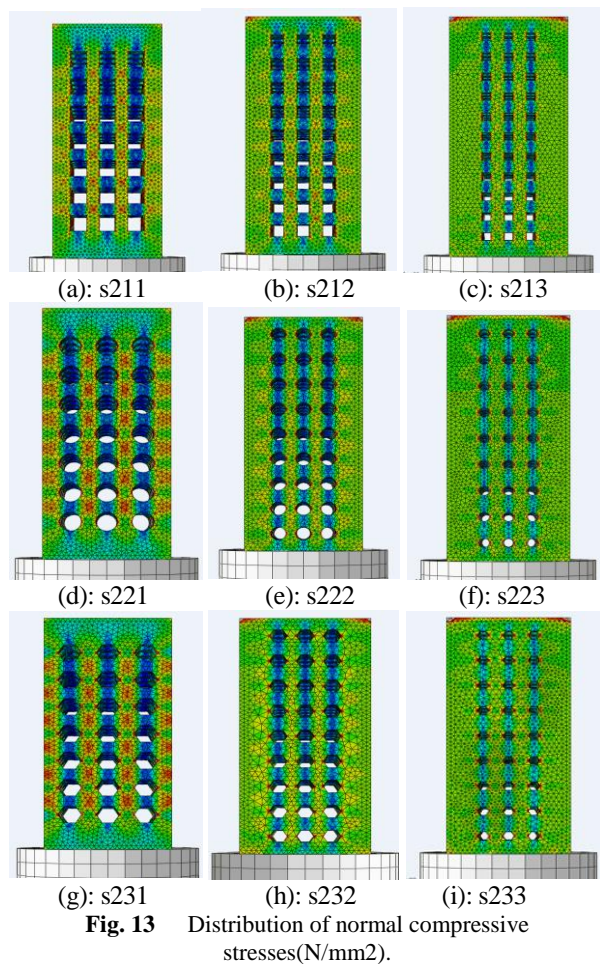


(b) the FE model of the porous cubic scaffolds

**Fig. 12** FEM details of porous cubic scaffold.

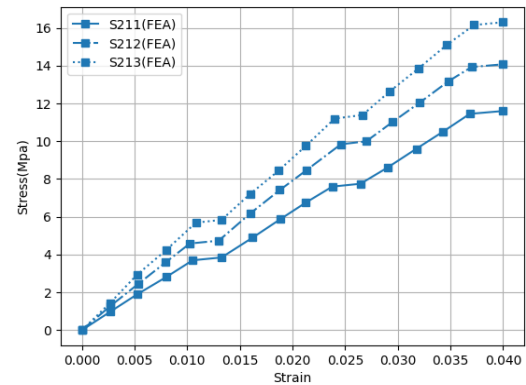
A Boundary Condition and FE model of the porous scaffolds are demonstrated in “Fig. 12”, a rigid body is attached to the upper surface of porous structures and the nodes in the bottom of the models were fully constrained. The rigid body movement being displaced of 10% compression to simulate the state of compression test. To avoid interpenetration, a frictionless general contact is defined between the porous structure and the rigid body. In simulation, model properties were set according to PLA with the density of 1.252 g/cm<sup>3</sup>, the elastic modulus of 3.5 Gpa and the Poisson’s ratio of 0.36 [33]. During the simulation process, the analysis

steps were dynamic and explicit. For the regular porous scaffold, the simulation was performed only in the Z-axis direction, but the anisotropy was considered for the irregular porous structure, and the simulation was performed along the X-, Y-, and Z-axes. Finally, the maximum Von Mises stress and effective elastic modulus, the average von Mises stress were recorded. The Finite Element Analysis (FEA) is introduced for verification and better comparison of experimental compressive test results of each specimen. Average stress of the finite element model node was applied for each sample in order to achieve better comparison of the compressive strength test. In the compressive test simulation of the porous structure when the strain is 0.1, as the average stress of all nodes increases, the ability of the model to resist deformation gets tougher. It means, the average stress of all nodes in the sample has mutual relationship with the model compressive strength affirmatively.

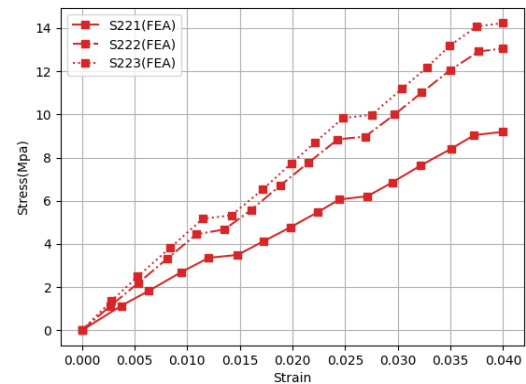


As can be seen from “Fig. 13”, which considers the stress distribution in scaffolds, on one hand, for comparison of the pore geometry, the stress is

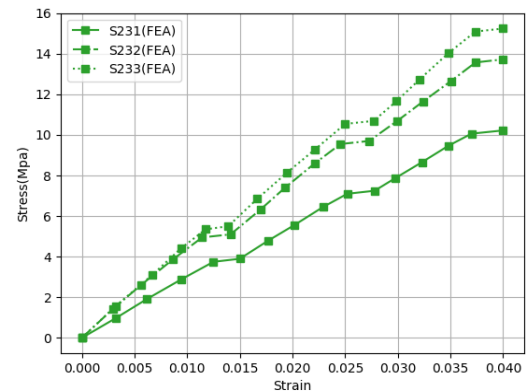
exceedingly concentrated around the pores of the cylinder and hexagonal pores compared with cubic pores. On the other hand, for comparison of the unit-cell porosity, with increasing porosity the stress is exceedingly concentrated in all geometries. In general, stress distribution of the porous scaffold is closely related to the porosity of the scaffold and the geometry of the unit-cells.



(a) Cube pore



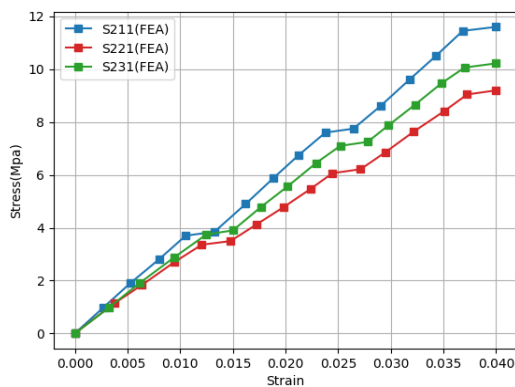
(b) Cylinder pore



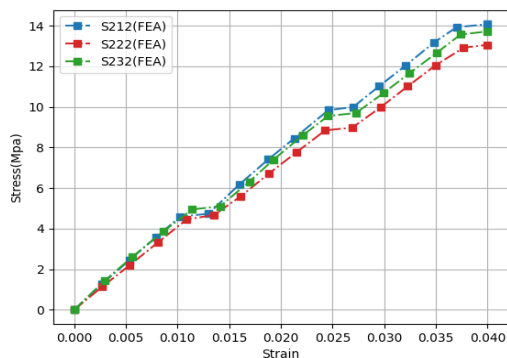
(c) Hexagonal prism pore

**Fig. 14** FEA stress–strain diagrams for same geometries and different porosities.

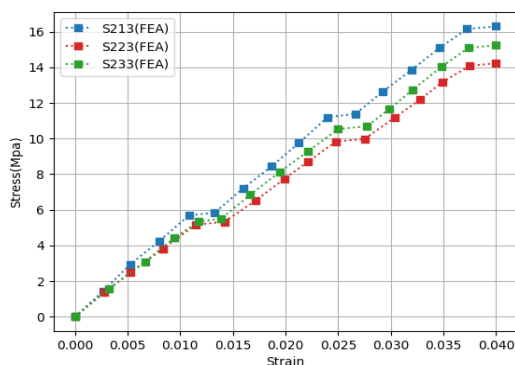
The stress–strain graphs from FEA, were similarly obtained by experimental compressive tests, from the force–displacement data recorded during the FEA. Figure 14, shows the stress–strain curves of porous cubic scaffolds under the same pore geometry and different porosities. Figure 15 shows the stress–strain curves of porous cubic scaffolds under different pore geometry and same porosities. Finally, Fig. 16 shows the stress–strain curves, overlapped for all specimens.



(a) 44% porosity



(b) 36% porosity



(c) 23% porosity

Fig. 15 FEA stress–strain diagrams for same porosities and different geometries.

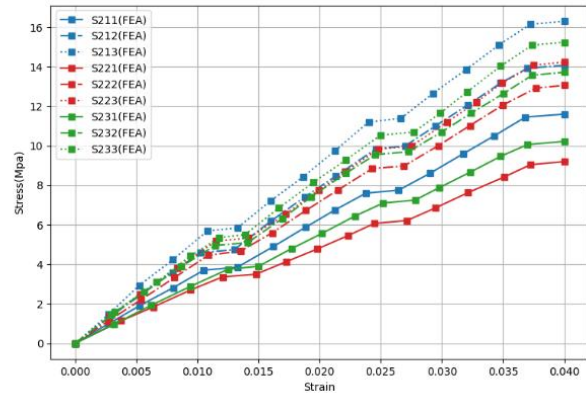


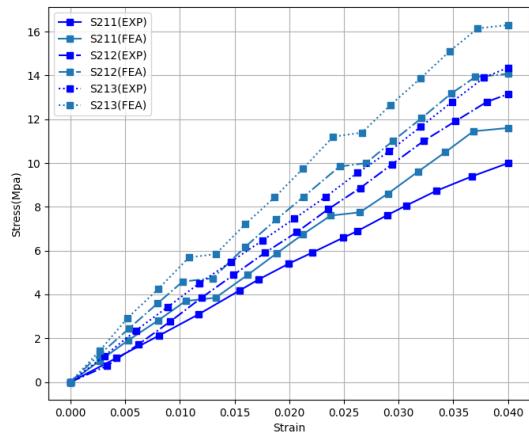
Fig. 16 FEA stress–strain curves.

As can be seen from “Fig. 14”, which considers the similar geometries, as the porosity decreases, the compressive strength of the porous scaffolds increases. Also, as can be seen from “Fig. 15”, which consider the similar porosities, cubic pore scaffolds (s211, s212 and s213) have the largest compressive strength over cylindrical and hexagonal ones. All the above results are clearly shown entirely in “Fig. 16” in order to compare all the specimens. Ultimate compressive strength and compressive elastic modulus were calculated similarly to the methodology followed for the experimental compressive tests. The results are shown in Table 6.

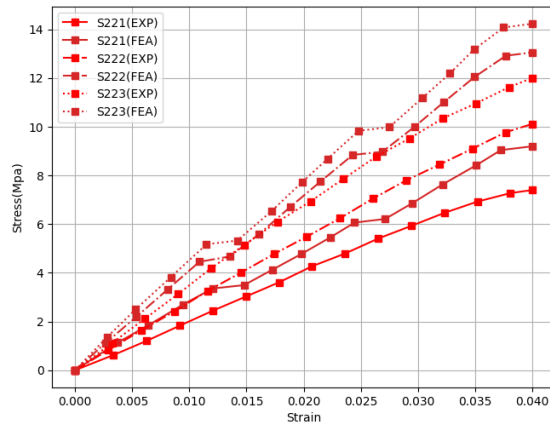
Table 6 Mechanical properties from FEA

Scaffold	E (Mpa)	$\sigma$ (Mpa)
S211	290	11.6
S212	352	14.1
S213	407	16.3
S221	230	9.2
S222	326	13.1
S223	356	14.2
S231	255	10.2
S232	343	13.7
S233	381	15.2

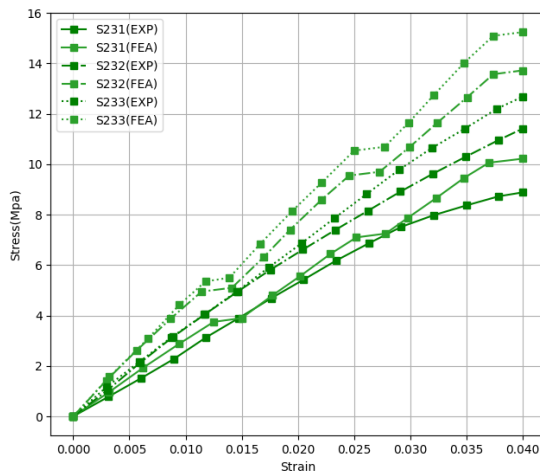
As seen from Table 6, in similar porosity, cubic pore scaffolds (s211, s212 and s213) results in higher compressive strength and modulus elasticity than the cylindrical and hexagonal ones and higher values belongs to the cubic pore scaffolds. In general, as the porosity decreases, the modulus of elasticity of the porous cubic scaffolds increases.



(a) Cube pore



(b) Cylinder pore



(c) Hexagonal prism pore

Fig. 17 Experimental Compressive stress–strain curves versus FEA stress–strain curves.

## 5 COMPARISON OF NUMERICAL AND EXPERIMENTAL RESULTS

As could be concluded from “Figs. 17 and 18”, which considers the FEA and experimental compressive tests results, in the case of geometry and porosity of scaffolds, the trend of stress-strain graphs of FEA and experimental compressive tests were completely similar for porous scaffolds, although the rate of diagram's changes were slightly different but the difference in results with an average error of 20% was acceptable.

Figure 18 shows Experimental Compressive stress–strain curves versus FEA stress–strain curves, overlapped for all specimens. It was noticeable that all the results obtained: Firstly, were in range of bone mechanical property for TE [36]. Secondly, FEA results, were consistent with experimental compressive test results, even though, the rates of change were slightly different but the difference in results with an average error of 20% was acceptable. These results are summarized as follows:

$$E_{\text{Cubic}} > E_{\text{Hexagonal prime}} > E_{\text{Cylinder}}$$

$$\sigma_{\text{Cubic}} > \sigma_{\text{Hexagonal prime}} > \sigma_{\text{Cylinder}}$$

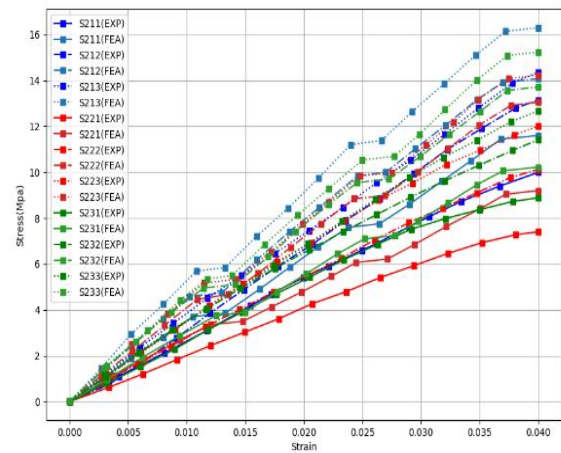


Fig. 18 Experimental Compressive stress–strain curves versus FEA stress–strain curves.

## 6 CONCLUSIONS

In this paper, nine porous scaffolds with different unit-cell geometry (cube, cylinder and hexagonal) were designed and fabricated by AM technology. Although, the mechanical properties results obtained for experimental compressive test and FEA, under different porosities, are quite consistent, however the rates of changes are slightly different. The significant findings are as follows:

1) The experimental compressive test and FEA, show that the porous scaffold is sensitive to the porosity and pore geometry. As the porosity increases, the compressive strength and modulus of elasticity obviously decreases in all geometry pore scaffolds. As the geometry changes in similar porosity, cubic pore scaffold achieved higher compressive strength and modulus of elasticity than cylinder and hexagonal prime.

2) The stress distribution of all porous scaffolds increased with increase in the porosity. In addition, stress concentration phenomena occurred as the porosity increases. Nevertheless, cubic pore scaffold has a more proper stress distribution than cylinder and hexagonal prime ones.

3) With regard to the modulus of elasticity and compressive strength tests for all nine porous scaffolds with three different porosities, for the three geometries of cube, cylinder and hexagonal prime, the maximum modulus of elasticity and compressive strength was observed in cubic pore with 23% porosity and the differences between cylinder and hexagonal pore with 23% porosity were not as significant as in the case of the modulus of elasticity.

In summary, the mechanical properties and porosity provide the requirements of the scaffold similar to human bone scaffold. In all of the nine porous scaffolds that were subjected to compressive test, the cubic pore scaffolds with 23% porosity (s213) and 33% porosity (s212) with respect to the compressive strength and porosity respectively, provide proper requirements of the TE.

---

## REFERENCES

- [1] Pina, S., Oliveira, J., and Reis, R., Natural- Based Nanocomposites for Bone Tissue Engineering and Regenerative Medicine: A Review, *Advanced Materials*, Vol. 27, No. 7, 1986, pp. 1143- 1169.
- [2] Bose, S., Vahabzadeh, S., and Bandyopadhyay A., Bone tissue engineering using 3D printing, *Materials Today*, Vol. 16, No. 12, 2013, pp. 496- 504.
- [3] Lichte, P., Pape, H., Pufe, T., Scaffolds for bone healing: concepts, *Materials and evidence Injury*, Vol. 42, No. 6, 2011, pp. 569- 573.
- [4] Polo-Corrales, L., Latorre-Esteves, M., and Ramirez-Vick, J.E., Scaffold design for bone regeneration, *Nanoscience and Nanotechnology*, Vol. 14, No. 1, 2014, pp. 15.
- [5] Roseti, L., Parisi, V., Petretta, M., Scaffolds for Bone Tissue Engineering: State of the art and new perspectives, *Mater Sci Eng C Mater Biol Appl*, Vol. 1, No. 78, 2017, pp. 1246- 1262.
- [6] Szojka, A., Lalh, K.H.J., Andrews, S., Biomimetic 3D printed scaffolds for meniscus tissue engineering, *Bioprinting*, Vol. 8, No. 1, 2017, pp. 1- 7.
- [7] Agarwal, R., and Garcia, J.A., Biomaterial strategies for engineering implants for enhanced osseointegration and bone repair, *Advanced Drug Delivery Reviews*, Vol. 1, No. 98, 2015, pp. 53- 62.
- [8] Guo, B., Lei, B., Li, P., Functionalized scaffolds to enhance tissue regeneration, *Regenerative biomaterials*, Vol. 1, No. 2, 2015, pp. 47- 57.
- [9] Wu, S., Liu, X., Yeung, K.W., Biomimetic porous scaffolds for bone tissue engineering, *Materials Science and Engineering: R: Reports*, Vol. 80, No. 1, 2014, pp. 1- 36.
- [10] Fereshteh, Z., Noeaid, P., Fathi, M., The effect of coating type on mechanical properties and controlled drug release of PCL/zein coated 45S5 bioactive glass scaffolds for bone tissue engineering, *Materials Science and Engineering : C*, Vol. 1, No. 54, 2015, pp. 50- 60.
- [11] Sadeghpour, S., Amirjani, A., Hafezi, M., Fabrication of a novel nanostructured calcium zirconium silicate scaffolds prepared by a freeze-casting method for bone tissue engineering, *Ceramics International*, Vol. 40, No. 10, 2014, pp. 16107- 16114.
- [12] Gentile, P., Chiono, V., Carmagnola, I., An overview of poly (lactic-co-glycolic) acid (PLGA)- based biomaterials for bone tissue engineering, *International journal of molecular sciences*, Vol. 3, No. 15, 2014, pp. 13640- 3659.
- [13] Rajzer, I., Menaszek, E., Kwiatkowski, R., Electrospun gelatin/poly ( $\epsilon$ -caprolactone) fibrous scaffold modified with calcium phosphate for bone tissue engineering, *Materials Science and Engineering : C*, Vol. 1, No. 44, 2014, pp. 183- 190.
- [14] Sadiasa, A., Nguyen, T.H., and Lee, B.T., In vitro and in vivo evaluation of porous PCL-PLLA 3D polymer scaffolds fabricated via salt leaching method for bone tissue engineering applications, *Journal of Biomaterials Science, Polymer*, Vol. 2, No. 25, 2013, pp. 150- 167.
- [15] Yeong, W.Y., Chua, C.K., Leong, K.F., Rapid prototyping in tissue engineering: challenges and potential, *Trends Biotechnol*, Vol. 22, No. 12, 2004, pp. 643- 652.
- [16] Vaezi, M., Seitz. H., and Yang, S. A., review on 3D micro-additive manufacturing technologies, *International Journal of Advanced Manufacturing Technology*, Vol. 1, No. 67, 2013, pp. 1721- 1754.
- [17] Leong, K.F., Cheah, C.M., and Chua, C.K., Solid freeform fabrication of three-dimensional scaffolds for engineering replacement tissues and organs, *Biomaterials*, Vol. 13, No. 24, 2003, pp. 2363- 2378.
- [18] Scott Crump S. Apparatus and method for creating three-dimensional objects. Patent 5121329, USA, 2014.

- [19] Upcraft, S., and Fletcher, R., The rapid prototyping technologies. *Materials Science, Assembly Automation*, Vol. 4, No. 23, 2003, pp. 318- 330.
- [20] Gómez, S., Vlad, M.D., Lopez, J., Design and properties of 3D scaffolds for bone tissue engineering, *Acta Biomater*, Vol. 1, No. 42, 2016, pp. 341- 350.
- [21] Williams, J.M., Adewunmi, A., Schek, R.M., Bone tissue engineering using polycaprolactone scaffolds fabricated via selective laser sintering, *Biomaterials*, Vol. 23, No. 26, 2005, pp. 4817- 4827.
- [22] Shuai, C., Mao, Z., Lu, H., Fabrication of porous polyvinyl alcohol scaffold for bone tissue engineering via selective laser sintering, *Biofabrication*, Vol. 1, No. 5, 2013, pp. 14- 15.
- [23] Eydivand, M.A., Hashjin, M.S, Farzad, A., Effect of technical parameters on porous structure and strength of 3D printed calcium sulfate prototypes, *Robotics and Computer-Integrated Manufacturing*, Vol. 37, No. 1, 2016, pp. 57- 67.
- [24] Farzadi, A., Waran, V., Hashjin, M.S., Effect of layer printing delay on mechanical properties and dimensional accuracy of 3D printed porous prototypes in bone tissue engineering, *Ceramics International*, Vol. 41, No. 1, 2015, pp. 8320- 8330.
- [25] Viana, T., Biscaia, S., Almeida, H.A., Permeability evaluation of laydown patterns and pore size of PCL scaffolds, *Procedia Engineering*, Vol. 59, No. 1, 2013, pp. 255- 262.
- [26] Feng, P., Meng, X., Chen, J.F., Mechanical properties of structures 3D printed with cementitious powders, *Construction and Building Materials*, Vol. 93, No. 1, 2015, pp. 486- 497.
- [27] Speirs, M., Hooreweder, B.V., Humbeeck, J.V., Fatigue behaviour of NiTi shape memory alloy scaffolds produced by SLM, a unit cell design comparison, *Journal of the Mechanical Behaviour of Biomedical Materials*, Vol. 70, No. 1, 2017, pp. 53- 59.
- [28] Kadkhodapour, J., Montazerian, H., Darabi, A.C., Failure mechanisms of additively manufactured porous biomaterials: effects of porosity and type of unit cell, *Journal of the Mechanical Behaviour of Biomedical Materials*, Vol. 50, No. 1, 2015, pp. 180- 191.
- [29] Bohner, M., Loosli, Y., Baroud, G., Commentary: deciphering the link between architecture and biological response of a bone graft substitute, *Acta biomaterial*, Vol. 7, No. 2, 2011, pp. 478- 484.
- [30] Liu, C., Xia, Z., and Czernuszka, J., Design and development of three-dimensional scaffolds for tissue engineering, *Chemical Engineering Research and Design*, Vol. 85, No. 7, 2007, pp. 1051- 1064.
- [31] Singhvi, M.S., Zinjarde, S.S., and Gokhale, D.V., Polylactic acid: Synthesis and biomedical applications, *Appl Microbiol*, Vol. 127, No. 1, 2019, pp. 1612- 1626.
- [32] ASTM D695-02a:2002. Standard Test Method for Compressive Properties of Rigid Plastic.
- [33] Farah, S., Anderson, D.G., and Langer, R., Physical and mechanical properties of PLA, and their functions in widespread applications - A comprehensive review, *Adv Drug Deliv Rev*, Vol. 107, No. 1, 2016, pp. 367- 392.
- [34] Stamboulis, Boccaccini, A.R., and Hench, L.L., Novel Biodegradable Polymer/Bioactive Glass Composites for Tissue Engineering Applications, *Advanced Engineering Materials*, Vol. 4, No. 3, 2002, pp. 105- 109.
- [35] Driscoll, S.B., *The Basics of Testing Plastics: Mechanical Properties, Flame Exposure, and General Guidelines*, Pennsylvania: Mayfield, 2004, p.25.
- [36] Goldstein, S.A., Wilson, D.L., Sonstegard, D.A., The mechanical properties of human tibial trabecular bone as a function of metaphyseal location, *Biomech*, Vol. 16, No. 1, 1983, pp. 965- 969.
- Hutmacher, D.W., Scaffolds in tissue engineering bone and cartilage, *Biomaterials*, Vol. 21, No. 24, 2000, pp. 2529- 2543.